Seismic anisotropy beneath the Eastern Dharwar craton

Sunil Kumar Roy, D. Srinagesh, Dipankar Saikia*, Arun Singh, and M. Ravi Kumar
NATIONAL GEOPHYSICAL RESEARCH INSTITUTE (COUNCIL OF SCIENTIFIC AND INDUSTRIAL RESEARCH), HYDERABAD 500007, INDIA

ABSTRACT

The southeastern Indian Shield, an assemblage of several Precambrian geological terranes, carries imprints of major tectonic events, including those related to rifting contemporaneous with India-Antarctica continental separation, volcanism, and sedimentation in Gondwana. In this study, we investigate the character of seismic anisotropy underneath 14 broadband stations spanning this region, utilizing the SK(K)S and direct S waves from earthquakes deeper than 400 km. In total, 113 high-quality splitting measurements reveal that the delay times (δt) between the fast and slow axes of anisotropy range from 0.32 s to 1.62 s for direct S waves and from 0.31 s to 1.80 s for SK(K)S phases. The fast polarization directions at a majority of the stations are in accordance with shear at the base of the lithosphere, coinciding with the present-day motion of the Indian plate with respect to the fixed Eurasian plate as defined through the NUVEL1A plate model. The coast-parallel splitting trends in the vicinity of the Eastern Ghat mobile belt can be reconciled by invoking a combination of anisotropy frozen in the lithosphere due to continental rifting along the eastern margin of the Indian plate and active asthenospheric anisotropy.

LITHOSPHERE; v. 4; no. 4; p. 259–268. | Published online 16 May 2012. doi: 10.1130/L198.1

INTRODUCTION

Shear-wave splitting is the most effective way to elucidate the nature of the crust and mantle anisotropy underneath a seismic station. It is widely accepted that the lattice-preferred orientation (LPO) of anisotropic minerals like olivine and orthopyroxene, which predominantly compose the upper mantle, is the primary cause of observed shear-wave splitting (Mainprice et al., 2000; Silver, 1996; Savage, 1999). This strain-induced LPO is considered to be a valuable indicator of past and/or present-day deformation (Babuška and Cara, 1991; Kay et al., 1999). The primary source of anisotropy in the crust can be envisaged in terms of stress-aligned fluid-filled cracks, microcracks, and preferentially oriented pore spaces (Crampin, 1994). Various seismic phases such as SK(K)S, PK(K)S, S, Sdiff, ScS, and Ps are used to investigate the intrinsic anisotropy of Earth utilizing shear-wave splitting, depending upon the tectonic region and the earthquake source receiver geometry. Anisotropy may be present in the lithosphere/sublithospheric mantle, in the midmantle region, and in the D″ layer, which extends 250–300 km above the core-mantle boundary (Fouch and Rondenay, 2006; Wookey and Kendall, 2004; Savage, 1999; Long, 2009). The lower mantle down to the core-mantle boundary above the D″ layer is generally considered to be isotropic (Silver, 1996; Savage, 1999; Long, 2009). Most models suggest that the D″ layer has transverse anisotropy with a vertical symmetry axis (VTI), but there is also evidence of complex anisotropy including tilted transverse anisotropy (TTI) and/or azimuthal anisotropy (Garnero et al., 2004; Maupin et al., 2005). SKS and SKKS have similar raypaths in the upper mantle, the only deviation being in the lowermost mantle. For an epicentral distance range of 100° to 120°, SKS and SKKS can generally be simultaneously identified for the same event-station pair. So any discrepancy in the splitting measurement of SKS and SKKS is probably related to the D″ anisotropy (Long, 2009; He and Long, 2011), under the assumption of horizontal axis of symmetry and neglecting differences in their angles of incidence.

In the Indian scenario, the first measurements of shear-wave splitting using SKS phases were made in the mid-1990s (Ramesh and Prakasam, 1995). These measurements have their limitations, considering the fact that most of them were made using analogue seismograms, although they were supplemented by a few measurements from short-period digital stations at HYB and GBA (Gauribidanur array) (Fig. 1) (Ramesh et al., 1996). Interestingly, the shear-wave splitting measurements using data from the GEOSCOPE station HYB (Fig. 1), located on the Eastern Dharwar craton, have revealed null results (Chen and Ozalaybey, 1998; Barruol and Hoffmann, 1999). Such null measurements were also reported at station SHIO (Shillong) (Fig. 1) in northeast India and at various stations south of the Indus-Tsangpo suture zone in southern Tibet (Chen and Ozalaybey, 1998; Sandvol et al., 1997; Fu et al., 2008; Singh et al., 2007). Based on these measurements, it was speculated that the onset of seismic anisotropy north of the Indus-Tsangpo suture zone could mark the termination of the Indian lithosphere beneath Asia. However, many splitting measurements from numerous broadband seismic stations installed during the past decade over diverse geological provinces of the Indian subcontinent (Singh et al., 2006, 2007; Kumar and Singh, 2008; Heintz et al., 2009; Kumar et al., 2010; Saikia et al., 2010; Mandal, 2011) testify to the anisotropic character of the Indian lithosphere and sublithospheric mantle and establish a dominance of the plate motion–related strain. Also, evidence for fossilized anisotropy, particularly in regions close to continental shear zones, is brought out in regions like the Southern granulite terrain and Cuddapah Basin. Heintz et al. (2009) presented the results of seismic anisotropy for 86 stations from the Himalayan arc to the southern Indian Peninsula and reiterated the source of anisotropy as due to shearing at the lithosphere-asthenosphere boundary. They suggested that this relative flow would create foliations in the horizontal plane, which get preserved in the lithosphere. Results of seismic anisotropy from 35 broadband stations in the Indian Shield using direct S waves show that the fast polarization azimuths are in agreement with those obtained from SKS splitting that indicate a predominance of strain related to absolute plate motion in the Indian Shield (Saikia et al., 2010).

Interestingly, although SK(K)S splitting at station HYB reveals null results, the splitting parameters obtained using direct S phases show fast-axis azimuths both in the NE and NNW-SSE directions (Saikia et al., 2010). In this context, it is relevant to investigate the anisotropic nature of the Eastern Dharwar craton in greater

*E-mail: dipankars@ngri.res.in

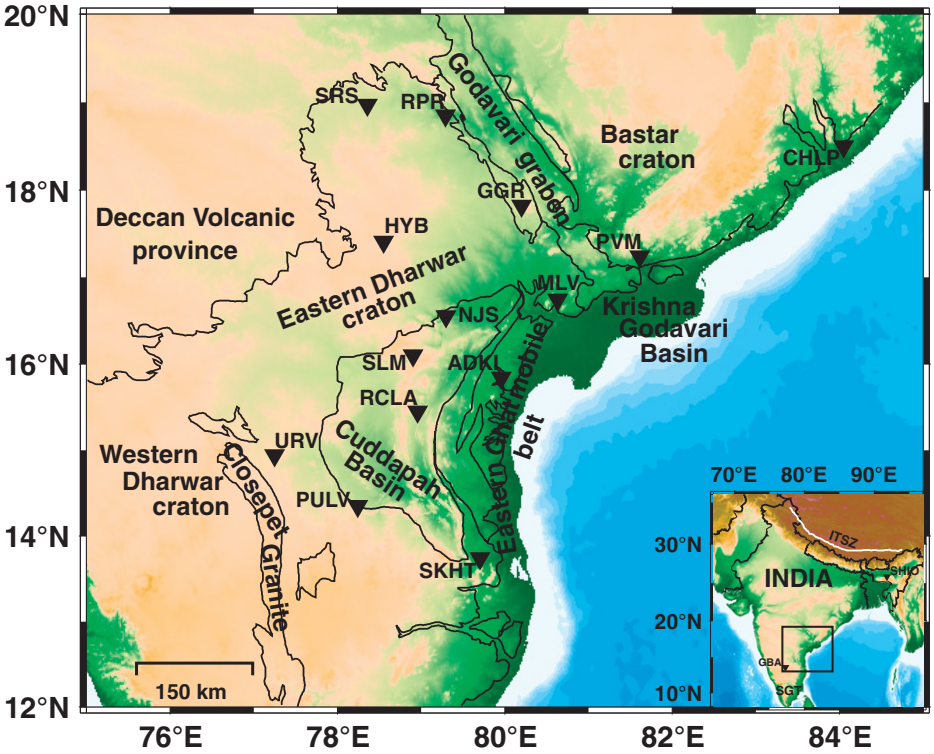

Figure 1. Map showing the location of 14 seismic stations (inverted triangles) and the station codes together with the geological provinces. Inset rectangle represents the study region, GBA—Gauribidanur array, SHIO—Shillong station, SGT—Southern granulite terrain, ITSZ—Indus-Tsangpo suture zone.

detail, to address issues like null anisotropy, the discrepancy between S and SK(K)S anisotropy, and possible presence of multiple layers of anisotropy that have an annihilating effect on each other. In this paper, we present new shear-wave splitting measurements at 14 broadband stations (Fig. 1) in the Eastern Dharwar craton and attempt to understand the characteristics of upper-mantle deformation beneath this region and examine whether the mantle beneath the region is isotropic as seen for station HYB or is anisotropic in nature akin to other tectonic regions of the Indian subcontinent. This study also presents a reanalysis of data from two stations, namely HYB and SLM, where the underlying medium was hitherto considered to be isotropic in nature. While wide ranges of back azimuths at HYB have revealed null measurements, a lack of consistency between the fast-axis azimuths and the back azimuth of the events has been reported for station SLM (Chen and Ozalaybey, 1998; Heintz et al., 2009).

GEOLOGY AND TECTONICS

The southeastern part of India is a juxtaposition of several tectonic elements comprising Archean, Proterozoic terranes, and younger sedimentary basins. The Archean blocks include the Eastern Dharwar craton and the Eastern Ghat mobile belt, while the sedimentary basins include the Proterozoic Cuddapah Basin, the Godavari graben, and the petroliferous Krishna-Godavari Basin (Ramam and Murty, 1997). The shield, being occupied by such sedimentary basins with ancestral cratonic blocks, led to the formation of crust composed of different geological entities, rifts, and faults, which resulted in the accumulation of stress and occasional release of strain energy. The Eastern Dharwar craton has experienced various episodes of tectonic deformation, the last one being a major kimberlitic event and characterized by Late Archean–Early Proterozoic cratonic growth with low-pressure metamorphism and remobilization of crustal blocks (Kumar et al., 1993; Ramam and Murty, 1997). The Eastern Dharwar craton is predominantly composed of granites and gneisses, with subordinate linear greenstone belts of limited dimensions, and there are series of linear and irregular Dharwar schist belts consisting mainly of volcanic rocks (Balakrishnan et al., 1990; Vasudev et al., 2000; Jayananda et al., 2000; Chadwick et al., 2000). The Cuddapah Basin, which punctures the Eastern Dharwar craton, is a prominent Proterozoic sedimentary basin in the Indian Shield (Ramakrishnan and Vaidyanadhan, 2008). It was formed due to the convergence between the Indian cratons and East Antarctica during the Proterozoic (Kumar and Leelanandam, 2008). The basin consists of igneous and sedimentary rocks of the Cuddapah and Kurnool Groups (Anand et al., 2003; Nagaraja Rao et al., 1987). To the east of the Cuddapah Basin, there lies the Eastern Ghat mobile belt, which is a juxtaposition of several terranes along longitudinal and transverse shear zones. The evolution of the Eastern Ghat mobile belt is associated with two distinct episodes of continental rifting, a first rifting event along the eastern margin of the Indian plate and then one along the eastern margin of the thickened arc crust (Kumar and Leelanandam, 2008). The mobile belt consists of pyroxene granulites, charnockites, migmatite gneisses, and supracrustal rocks (Paul et al., 1990). The region between the Cuddapah Basin and the Eastern Ghat mobile belt is often characterized as a suture zone (Gibb and Thomas, 1976). The NW-SE trending Godavari graben is an intracratonic basin filled with Gondwana sediments of variable thickness. The graben that separates the Eastern Dharwar craton and the Bastar craton has been a site of repeated episodes of rifting and convergence (Biswas, 2003). One important feature of this graben is the absence of igneous intrusions, suggestive of a passive rift (Olsen and Morgan, 1995). Several studies have been conducted to elucidate the lithospheric thickness of this part of the Indian Shield. While the results from surface-wave tomography (Mitra et al., 2006) suggest a thickness of ~155 km for the Indian lithosphere, modeling of S receiver functions yields only a 100-km-thick lithosphere (Kumar et al., 2007). However, it is now argued that the cratonic segment of the south Indian Shield is thinner compared to the other Archean cratons of the world.

DATA AND METHODS

Data accrued from a network of 14 broadband seismic stations (Fig. 1; Table 1) being operated by the National Geophysical Research Institute (NGRI) spanning the period September 2008 to September 2011 are used in this study. The units include REFTEK broadband FBS-3 sensors (120 s, 50 Hz) and REFTEK 130-01 DAS recorders (24 bit) time tagged with global positioning system (GPS) data. Waveforms of 73 earthquakes (Fig. 2) having magnitude ≥5.5, within an epicentral distance range of 85° to 120° (for SK[K]S) and 40° to 80° (for direct S) were used for splitting analysis. While dealing with the S phases, the contribution of source side anisotropy was minimized by restricting the focal depths of the events to >400 km. Waveforms

TABLE 1. DETAILS OF THE SEISMIC STATIONS USED IN THIS STUDY

Station code	Latitude (°E)	Longitude (°N)	Sensor type	Geological unit
ADKI	15.84	79.96	REF TEK 151	EGMB
CHLP	18.50	84.05	REF TEK 151	EGMB
GGR	17.82	80.20	REF TEK 151	GG
HYB	17.41	78.55	REF TEK 151	EDC
MLV	16.74	80.63	REF TEK 151	EGMB
NJS	16.55	79.30	REF TEK 151	CB
PULV	14.35	78.24	KS2000	EDC
PVM	17.24	81.61	REF TEK 151	EGMB
RCLA	15.45	78.96	REF TEK 151	CB
RPR	18.85	79.29	REF TEK 151	EDC
SKHT	13.74	79.70	REF TEK 151	EGMB
SLM	16.10	78.90	REF TEK 151	CB
SRS	18.97	78.36	REF TEK 151	EDC
URV	14.94	77.25	REF TEK 151	EDC

Note: Abbreviations: EGMB—Eastern Ghat mobile belt; GG—Godavari graben, EDC—Eastern Dharwar craton; CB—Cuddapah Basin.

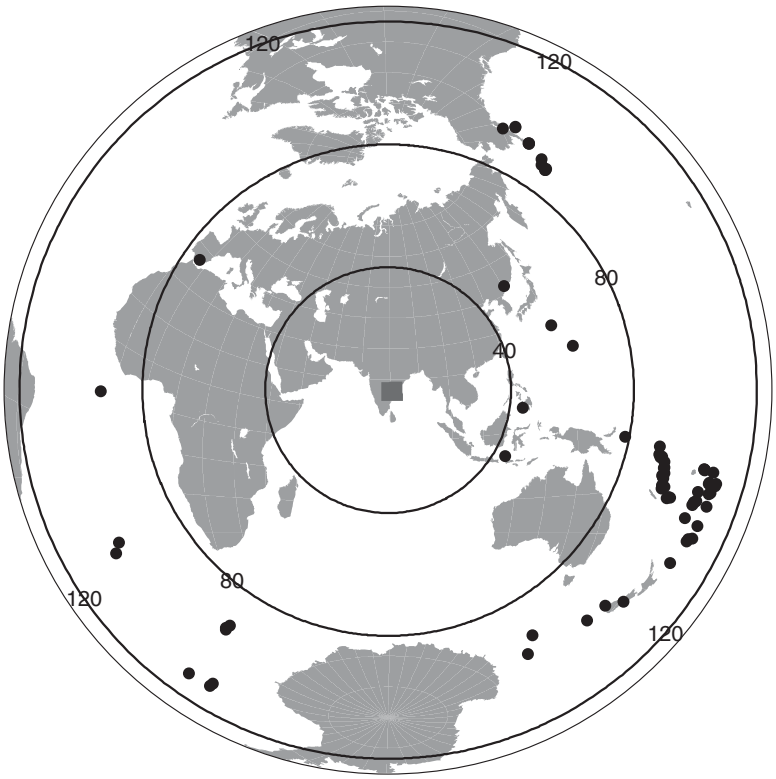

Figure 2. Epicentral locations of the 73 teleseismic events used in this study. The study region is indicated by a filled square. The center of the circles indicating epicentral distances is at 16.55°N, 79.30°E.

corresponding to the phases of interest were extracted based on the theoretical traveltimes computed using the IASP91 Earth reference model (Kennett and Engdahl, 1991). After performing quality analysis, only those waveforms with high signal-to-noise ratio (S/N > 5) as well as clear arrival of the relevant shear-wave phase were retained for further analysis. To enhance the dominant period of SK(K)S phases and to suppress the effects of noise, the data were filtered using a Butterworth band-pass filter between 4 s and 20 s. In order to avoid contamination of the direct S waves with other phases like PcS, ScPmP, SP, and PL, which arrive in close proximity (for details, see Saikia et al., 2010), the analysis was performed using raw (unfiltered) data. Whenever filtering became imperative, a series of Butterworth filters was used by changing one end from 1 to 5 s while keeping the other end fixed at 50 s. Eventually, only those measurements that produced stable splitting results for different filters were considered.

In order to quickly assess the quality of splitting estimates, namely, the fast polarization azimuth (Φ) and delay time (δt), and identify the null measurements, we first used the SplitLab analysis software (Wüstefeld et al., 2008), which combines both the Silver and Chan (1991) approach to minimize energy on the transverse component, and the rotation-correlation approach (Bowman and Ando, 1987), since it can handle large data sets and minimize the time taken for analysis. Subsequently, we selected the good-quality waveforms that exhibited clear splitting and also those that showed null measurements. We then applied the Teanby shear-wave splitting analysis code to those events that gave consistent results from both the methods in order to estimate the splitting parameters.

The cluster analysis method of Teanby et al. (2004), which is based on the algorithm of Silver and Chan (1991), obtains an optimum solution by performing a grid search over Φ and δt to minimize the second eigenvalue of the covariance matrix for the particle motion over a range of window lengths. The advantage of this method is that it automates window selection, makes different ranges of measurements around the relevant phase, and applies cluster analysis to identify the most stable result. For a given event-station pair, the authenticity of the parameter estimation involves the following criteria: (1) clarity of the radial and transverse components of the waveforms, (2) ellipticity of the initial particle motion, (3) linearity of particle motion after correction, (4) similarity of the fast and slow components after correction, and (5) unique as well as a well-defined error surface. Figure 3 demonstrates an example showing the SKS spitting analysis at station RPR. The analysis can sometimes lead to a particular category of estimate called the "null" measurement, when the shear-wave propagates through an isotropic medium or if the initial polarization coincides with either the fast or slow axis or in the presence of multiple layers of anisotropy with different orientations and strengths. In such situations, the shear wave does not exhibit splitting, and there would not be any energy on the transverse component, or the particle motion is linear before the anisotropy correction.

SPLITTING RESULTS

The shear-wave splitting measurement procedure yielded 113 (Table 2) well-constrained

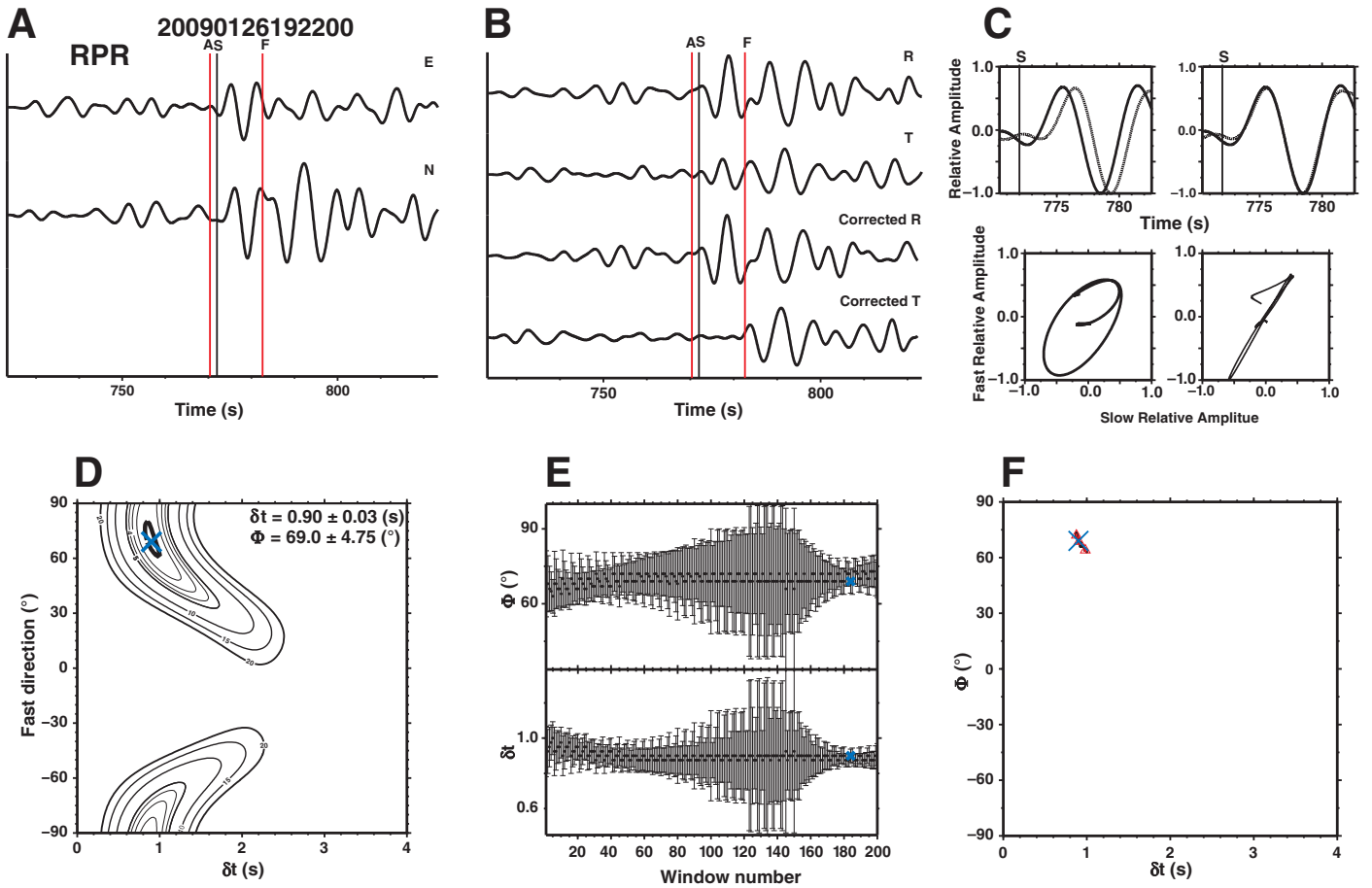

Figure 3. Example of an SKS splitting measurement performed for an event at station RPR. (A) Original N and E components showing the phase picking. Vertical lines A and F indicate the start and end times of the shear-wave analysis window, while the vertical line S represents the SKS wave pick. (B) Radial (R) and transverse (T) components, uncorrected (top) and splitting corrected (bottom). (C) Waveforms (top) and particle motion (bottom) of fast and slow waves before and after correction for anisotropy. (D) Contour plot of the energy in the transverse component. Minimum energy is shown as a cross with 95% confidence region (thick contour). (E) Measurement of Φ and δ*t* from all the windows on which shear-wave splitting analysis was performed. (F) Φ vs. δ*t* values (triangles) obtained for various windows used for cluster analysis. The best solution (with the lowest variance) is indicated by a cross.

individual measurements of Φ and δ*t* using SK(K)S and direct S phases. These include 24 measurements of direct S phases. Histograms of the delay times between the fast and slow axis tend to cluster around 0.8 s (Fig. 4), which is slightly lower than that observed globally for continental shields (~1 s). The delay times are not so consistent and vary between 0.31 s and 1.80 s for SK(K)S phases and between 0.32 s and 1.62 s for direct S waves. The individual splitting measurements at each station have been plotted over a topographic map (Fig. 5A), and a similar plot of all the well-constrained null measurements (69 in total) is shown in Figure 5B.

The orientations of the fast polarization azimuth for stations ADKI, CHLP, MLV, RCLA, PULV, and RPR obtained using both SK(K)S and S waves are aligned close to the NNE-SSW direction, which is parallel to the motion of Indian plate as defined through the NUVEL1A model by considering a fixed Eurasian plate (DeMets et al., 1994). A slightly different fast polarization azimuth (NE) is obtained for station GGR using both SK(K)S and S waves. At station PVM in the Eastern Ghat mobile belt, the SK(K)S splitting direction is oriented ENE-WSW, while the S-wave splitting yields both NNE-SSW and NE directions. Such a discrepancy is also observed at stations NJS and SLM in the Cuddapah Basin, where the SK(K)S splitting directions are in the ENE-WSW direction and the S-wave fast polarization azimuth is in the NE direction.

The deviations in the anisotropic directions of SK(K)S and S waves are probably due to the fact that the S waves sample a very different path compared to the core-refracted SK(K)S phase. The observed fast polarization azimuth at station SLM, although indicates a dominant ENE-WSW–oriented anisotropy, requires more observations to validate the apparently isotropic behavior reported earlier (Heintz et al., 2009). For SRS and URV, the splitting directions are NNW-SSE and NNE-SSW both for SK(K)S and S phases, i.e., close to the relative motion of the Indian plate with respect to a fixed Eurasian plate (DeMets et al., 1994) (NNE-SSW) or through the HS3-NUVEL1A model to fixed hotspot frame (Gripp and Gordan, 2002) (NNW-SSE).

The large scatter in Φ observed for SKHT (in Eastern Ghat mobile belt) and lack of consistency with back azimuths of the events are characteristic of an apparently isotropic medium (similar to the result reported for the station SLM by Heintz et al., 2009) or are related to vertical variations in anisotropy (e.g., Silver and Savage, 1994) or are related to complex anisotropy (Booth et al., 1985; Babuška et al., 1993). The well-constrained null measurements

TABLE 2. INDIVIDUAL SPLITTING PARAMETERS, ALONG WITH THEIR UNCERTAINTIES, OBTAINED USING EVENTS AT DIFFERENT STATIONS AS INDICATED

Event date (mm/dd/yy)	Phase	Back azimuth (°)	Distance (°)	ϕ (°)	δt (s)	Polarization (°)	Depth (km)	Quality
ADKI								
11/07/08	SKKS	104.9	88.2	24 ± 9.50	1.35 ± 0.31	94.9	–	G
03/04/10	SKS	103.9	105.0	22 ± 6.50	0.90 ± 0.20	95.6	–	F
04/11/10	S	305.0	75.3	34 ± 11.00	0.50 ± 0.08	72.7	609	G
10/16/10	SKS	106.3	110.3	–78	–	–	–	N
01/05/11	SKS	111.2	97.4	5	–	–	–	N
01/23/11	SKS	106.7	108.0	–79	–	–	–	N
02/07/11	S	101.1	77.9	40 ± 15.50	0.92 ± 0.35	155.1	428	F
04/18/11	SKS	121.8	106.8	28	–	–	–	N
06/24/11	SKS	35.8	88.2	57 ± 10.50	0.92 ± 0.12	24.3	–	G
07/29/11	SKKS	110.8	105.0	47 ± 19.75	0.77 ± 0.33	114.6	–	F
07/29/11	SKS	110.8	105.0	15	–	–	–	N
CHLP								
11/04/08	SKS	108.0	101.7	28 ± 9.00	0.97 ± 0.26	99.7	–	F
09/29/08	SKS	116.7	106.0	31	–	–	–	N
12/09/08	SKS	107.0	101.5	24 ± 10.5	1.00 ± 0.34	101.5	–	F
08/05/09	SKS	135.5	97.9	50	–	–	–	N
11/08/09	SKS	106.9	99.9	29 ± 12.25	0.87 ± 0.23	99.9	–	G
11/22/09	SKS	104.8	104.0	40 ± 5.00	0.70 ± 0.08	104.0	–	G
12/09/09	SKS	112.1	109.1	38 ± 15.70	0.85 ± 0.31	109.1	–	F
01/15/09	SKS	112.3	108.4	46 ± 17.25	1.15 ± 0.27	108.4	–	F
02/07/10	SKS	110.7	108.9	61 ± 13.25	0.82 ± 0.12	108.8	–	F
03/08/10	S	78.5	57.0	–38 ± 7.25	0.40 ± 0.05	112.4	457	G
01/31/11	SKS	108.3	106.1	26 ± 2.75	1.55 ± 0.18	102.3	–	G
02/21/11	SKS	113.8	101.8	42 ± 3.25	0.95 ± 0.11	113.7	–	G
04/03/11	SKKS	104.7	102.2	56 ± 5.75	0.82 ± 0.03	97.6	–	F
04/03/11	SKS	104.7	102.2	39 ± 2.50	0.72 ± 0.04	105.3	–	F
04/05/11	SKS	104.7	102.2	37 ± 6.00	0.92 ± 0.12	102.7	–	G
07/29/11	SKKS	111.1	102.3	45 ± 1.50	0.80 ± 0.02	111.5	–	G
07/29/11	SKS	111.1	102.3	40 ± 2.50	0.90 ± 0.07	109.9	–	G
GGR								
02/07/11	S	101.6	78.1	46 ± 7.50	0.97 ± 0.18	163.1	414	G
04/03/11	SKS	103.9	105.6	66 ± 5.00	0.80 ± 0.03	116.5	–	G
05/05/11	SKKS	30.1	91.0	74 ± 10.25	0.80 ± 0.08	34.0	–	F
05/10/11	SKKS	109.9	94.3	53 ± 2.50	1.15 ± 0.08	119.3	–	G
07/29/11	SKS	110.4	105.9	78 ± 18.25	0.52 ± 0.19	123.5	–	F
09/15/11	SKS	107.9	105.9	61 ± 6.75	0.82 ± 0.08	119.0	–	F
HYB								
10/22/08	SKKS	103.7	110.2	–74	–	–	–	N
11/07/08	SKS	104.3	93.9	16	–	–	–	N
11/14/08	SKS	213.8	92.7	–50	–	–	–	N
11/22/08	SKS	296.6	92.7	–4	–	–	–	N
12/09/08	SKS	105.4	94.3	–71	–	–	–	N
12/17/08	SKS	103.7	107.2	–74	–	–	–	N
12/20/08	SKS	240.4	100.4	52	–	–	–	N
02/28/09	SKS	211.0	111.6	29	–	–	–	N
04/16/09	SKKS	211.2	112.6	–51	–	–	–	N
06/12/09	SKS	107.0	94.5	–69	–	–	–	N
06/16/09	SKS	213.9	94.4	32	–	–	–	N
08/05/09	SKS	134.6	100.8	–41	–	–	–	N
11/18/09	SKS	214.1	94.0	3 ± 7.50	0.72 ± 0.06	37.1	–	G
11/22/09	SKS	103.8	107.2	–72	–	–	–	N
02/18/10	S	48.8	50.7	37 ± 9.25	0.75 ± 0.13	159.4	577	F
03/08/10	S	76.8	62.4	–37 ± 6.00	0.40 ± 0.03	110.6	457	G
03/04/10	SKS	103.4	92.7	19	–	–	–	N
04/10/10	SKS	105.7	109.7	–72	–	–	–	N
04/12/10	SKS	149.1	93.6	52 ± 11.50	1.02 ± 0.33	154.9	–	G
05/27/10	SKS	103.7	92.1	–72	–	–	–	N
09/03/10	SKS	131.5	104.3	–46	–	–	–	N
10/16/10	SKS	105.4	112.0	–71	–	–	–	N
01/31/11	SKS	107.4	110.7	–73	–	–	–	N
02/21/11	SKS	112.9	106.1	29	–	–	–	N
04/03/11	SKS	109.7	107.0	–74	–	–	–	N
04/18/11	SKS	121.2	108.8	39	–	–	–	N
05/10/11	SKS	109.5	95.6	42	–	–	–	N
07/29/11	SKS	110.1	106.9	–71	–	–	–	N

(*continued*)

TABLE 2. INDIVIDUAL SPLITTING PARAMETERS, ALONG WITH THEIR UNCERTAINTIES, OBTAINED USING EVENTS AT DIFFERENT STATIONS AS INDICATED (*continued*)

Event date (mm/dd/yy)	Phase	Back azimuth (°)	Distance (°)	ϕ (°)	δt (s)	Polarization (°)	Depth (km)	Quality
MLV								
10/16/10	SKS	106.1	110.0	28	–	–	–	N
01/23/11	SKS	106.5	107.7	23	–	–	–	N
02/02/11	SKKS	30.2	91.7	47 ± 8.00	1.27 ± 0.26	26.2	–	F
02/07/11	S	101.5	77.5	23 ± 12.50	0.80 ± 0.14	163.5	414	G
02/21/11	SKS	113.4	104.0	33	–	–	–	N
04/03/11	SKS	104.3	104.9	47 ± 16.50	0.42 ± 0.18	113.4	–	F
04/18/11	SKS	121.6	106.8	30	–	–	–	N
NJS								
01/18/09	SKKS	116.7	108.9	65 ± 19.25	0.47 ± 0.22	116.5	–	F
02/18/09	SKKS	113.6	109.9	84 ± 05.50	0.52 ± 0.02	125.6	–	F
03/30/09	SKS	26.0	95.0	86 ± 18.00	0.37 ± 0.18	207.4	–	F
06/16/09	SKS	214.0	94.1	–50	–	–	–	N
08/05/09	SKS	134.7	99.6	51	–	–	–	N
10/11/09	SKS	103.4	90.7	17	–	–	–	N
02/07/10	SKKS	110.0	106.1	71 ± 14.50	0.57 ± 0.10	113.6	–	F
02/18/10	S	48.0	50.6	11 ± 17.50	0.77 ± 0.26	158.6	577	F
02/19/10	SKKS	107.6	110.0	46 ± 21.00	0.95 ± 0.19	101.8	–	F
03/04/10	SKS	103.6	91.8	18	–	–	–	N
03/08/10	S	76.5	61.9	–27 ± 18.50	0.32 ± 0.12	115.5	457	F
12/26/10	SKS	109.1	94.6	23	–	–	–	N
02/07/11	S	101.1	78.7	4 ± 19.75	1.05 ± 0.35	157.5	414	F
04/03/11	SKS	104.1	106.1	–80	–	–	–	N
07/06/11	SKKS	115.7	110.4	76 ± 11.25	0.40 ± 0.06	124.7	–	F
10/04/11	S	68.5	57.3	–32 ± 13.25	0.50 ± 0.16	124.3	455	G
10/25/11	SKS	35.5	88.0	–74 ± 3.50	1.07 ± 0.12	33.7	–	F
PULV								
11/22/09	SKKS	104.5	106.7	27 ± 7.00	1.12 ± 0.20	96.4	–	F
02/18/10	S	47.0	52.8	23 ± 10.25	0.95 ± 0.16	148.2	574	F
12/25/10	SKKS	109.0	94.4	–77	–	–	–	N
02/21/11	SKS	113.6	105.2	–72	–	–	–	N
07/29/11	SKS	110.9	106.1	–73	–	–	–	N
PVM								
09/08/08	SKS	109.6	93.5	66 ± 18.25	0.42 ± 0.17	106.7	–	F
11/04/08	SKS	107.1	92.0	62 ± 14.00	0.57 ± 0.12	101.1	–	F
06/02/09	SKS	107.9	91.7	79 ± 22.75	0.72 ± 0.58	113.1	–	F
04/01/10	SKS	152.3	96.7	61 ± 4.0	1.22 ± 0.20	164.8	–	G
07/23/10	S	99.2	42.1	19 ± 3.00	0.80 ± 0.05	82.6	607	G
09/03/10	SKS	132.0	102.0	44	–	–	–	N
12/26/10	SKKS	110.0	92.6	–80 ± 5.75	1.22 ± 0.11	131.3	–	G
12/28/10	SKS	110.4	104.3	76 ± 9.75	0.80 ± 0.05	121.9	–	G
01/05/11	SKS	111.4	96.4	62 ± 6.50	0.85 ± 0.10	119.7	–	G
02/07/11	S	102.0	76.7	60 ± 7.50	1.55 ± 0.33	170.3	414	F
03/06/11	SKS	215.2	114.5	41	–	–	–	N
03/10/11	S	121.7	42.2	38 ± 4.50	0.70 ± 0.12	111.0	510	F
04/03/11	SKS	104.4	104.1	86 ± 9.75	0.85 ± 0.18	111.7	–	F
05/10/11	SKKS	110.3	92.8	58 ± 7.58	0.67 ± 0.05	111.9	–	F
09/09/11	SKS	19.2	108.6	55 ± 9.75	0.87 ± 0.10	16.3	–	G
10/25/11	SKS	36.1	86.1	–89 ± 9.25	0.52 ± 0.05	40.3	–	G
11/05/11	SKS	108.4	92.3	74 ± 6.75	0.97 ± 0.10	111.8	–	F
RCLA								
02/18/10	S	47.4	78.8	29 ± 16.50	1.12 ± 0.41	142.7	414	F
03/04/10	SKS	103.4	91.8	44 ± 14.75	0.42 ± 0.15	102.1	–	F
03/08/10	S	75.9	62.6	–63 ± 12.00	0.60 ± 0.21	107.1	457	G
04/11/10	S	305.0	75.03	45 ± 06.25	0.95 ± 0.17	66.1	609	G
05/27/10	SKS	103.9	91.3	–86	–	–	–	N
09/03/10	SKS	131.9	102.7	40	–	–	–	N
10/16/10	SKKS	106.2	111.1	22	–	–	–	N
04/03/11	SKS	104.3	106.1	60 ± 3.00	0.62 ± 0.08	76.9	–	F
07/29/11	SKKS	110.7	105.0	21 ± 7.00	0.95 ± 0.10	88.1	–	G
07/29/11	SKS	110.7	105.0	67 ± 12.00	0.62 ± 0.23	82.1	–	F
RPR								
01/26/09	SKS	35.7	86.3	69 ± 5.50	0.90 ± 0.05	211.2	–	G
01/05/11	SKS	110.0	99.0	84 ± 10.00	0.77 ± 0.08	123.5	–	F
02/21/11	SKKS	112.6	106.0	68 ± 6.25	1.07 ± 0.06	122.5	–	G

(*continued*)

TABLE 2. INDIVIDUAL SPLITTING PARAMETERS, ALONG WITH THEIR UNCERTAINTIES, OBTAINED USING EVENTS AT DIFFERENT STATIONS AS INDICATED (*continued*)

Event date (mm/dd/yy)	Phase	Back azimuth (°)	Distance (°)	ϕ (°)	δt (s)	Polarization (°)	Depth (km)	Quality
03/06/11	SKS	215.8	114.6	36	–	–	–	N
03/10/11	S	121.3	45.0	53 ± 13.00	0.60 ± 0.20	117.3	508	G
07/29/11	SKKS	109.9	106.7	44 ± 4.25	1.20 ± 0.19	116.4	–	G
SKHT								
01/24/09	SKS	24.0	95.4	–81 ± 1.25	1.60 ± 0.04	30.9	–	F
02/18/09	SKKS	114.5	108.4	40 ± 5.00	1.80 ± 0.22	108.7	–	F
03/30/09	SKS	26.2	97.3	43 ± 4.75	1.17 ± 0.15	211.3	–	G
04/16/09	SKS	210.5	110.1	–52	–	–	–	N
06/16/09	SKS	214.2	92.0	21 ± 15.75	1.02 ± 0.35	45.1	–	F
10/31/09	SKS	101.7	89.5	17 ± 23.25	1.57 ± 0.53	89.6	–	F
11/22/09	SKS	104.9	105.2	–88 ± 9.25	0.47 ± 0.12	107.5	–	F
12/09/09	SKS	111.1	96.2	76 ± 18.75	0.72 ± 0.26	115.3	–	F
07/18/10	SKS	34.6	91.0	–71 ± 17.50	1.10 ± 0.43	39.6	–	F
02/07/11	S	100.6	77.8	64 ± 7.50	1.62 ± 0.40	172.8	414	F
03/22/11	SKS	238.5	102.1	29 ± 7.25	0.72 ± 0.09	59.0	–	F
05/05/11	SKKS	29.9	94.6	–77 ± 7.50	0.72 ± 0.08	45.4	–	F
SLM								
01/15/09	SKS	111.2	97.6	–75	–	–	–	N
03/30/09	SKS	25.8	95.5	67 ± 6.25	0.62 ± 0.03	20.8	–	G
10/13/09	SKS	33.7	90.7	59 ± 16.75	0.80 ± 0.23	30.3	–	F
10/25/09	SKKS	109.6	106.9	36 ± 9.75	0.85 ± 0.16	100.8	–	G
11/22/09	SKKS	104.1	106.5	83 ± 18.50	0.47 ± 0.21	110.9	–	F
12/09/09	SKKS	110.7	97.8	19 ± 17.75	1.20 ± 0.50	93.2	–	F
02/07/10	SKKS	110.2	106.3	26	–	–	–	N
03/04/10	SKS	103.5	92.1	–84	–	–	–	N
02/02/11	SKKS	29.6	93.1	57 ± 16.25	0.87 ± 0.28	31.8	–	F
02/21/11	SKKS	113.3	105.3	35 ± 4.00	1.50 ± 0.28	112.5	–	F
04/03/11	SKKS	104.1	106.4	83 ± 18.00	0.42 ± 0.20	107.7	–	F
05/05/11	SKKS	29.6	92.9	71 ± 3.75	0.80 ± 0.02	30.2	–	G
07/29/11	SKKS	110.6	106.1	31 ± 1.25	1.65 ± 0.10	111.0	–	F
07/29/11	SKS	110.6	106.1	–71	–	–	–	N
10/25/11	SKS	35.4	88.6	86 ± 17.75	0.75 ± 0.21	29.8	–	G
SRS								
12/17/08	SKS	103.1	107.8	–40 ± 16.00	0.52 ± 0.15	101.8	–	F
03/30/09	SKS	25.4	93.2	–69	–	–	–	N
04/16/09	SKKS	211.7	113.8	–45 ± 4.25	1.20 ± 0.16	26.8	–	F
04/16/09	SKS	211.7	113.8	–2 ± 17.25	0.45 ± 0.16	30.8	–	F
05/16/09	SKS	25.6	93.3	30	–	–	–	N
06/12/09	SKS	106.9	95.0	11	–	–	–	N
11/02/09	SKKS	109.0	112.2	–78	–	–	–	N
11/02/09	SKS	109.0	112.2	–54 ± 17.00	0.85 ± 0.27	100.3	–	F
11/18/09	SKS	214.3	95.2	9 ± 17.25	0.42 ± 0.16	39.4	–	F
11/22/09	SKKS	103.2	107.7	7	–	–	–	N
11/24/09	SKKS	105.1	112.4	–77	–	–	–	N
02/07/10	SKKS	109.2	107.8	–69	–	–	–	N
03/08/10	S	77.6	62.2	–56 ± 02.75	0.80 ± 0.11	111.8	457	G
12/28/10	SKKS	109.3	107.8	15	–	–	–	N
03/06/11	SKKS	215.8	114.1	4 ± 6.00	0.75 ± 0.05	39.5	–	G
03/06/11	SKS	215.8	114.1	–31 ± 16.00	0.47 ± 0.19	34.2	–	F
03/10/11	S	120.7	45.8	9 ± 20.75	1.07 ± 0.46	109.6	508	F
04/03/11	SKKS	103.1	107.5	4	–	–	–	N
04/03/11	SKS	103.1	107.5	7 ± 0.75	1.32 ± 0.06	105.3	–	F
08/24/11	SKS	107.4	95.2	–65	–	–	–	N
09/03/11	SKS	109.2	97.7	–72	–	–	–	N
10/25/11	SKS	35.3	86.5	–47	–	–	–	N
URV								
02/18/09	SKS	114.1	111.1	30	–	–	–	N
08/05/09	SKS	134.5	99.9	–1 ± 20.00	0.50 ± 0.42	141.0	–	F
12/09/09	SKS	110.8	99.0	16 ± 17.50	1.10 ± 0.43	119.0	–	F
03/04/10	SKS	103.0	93.3	–58 ± 11.00	0.47 ± 0.17	105.3	–	F
03/08/10	S	75.4	64.3	–24 ± 7.00	0.52 ± 0.04	116.1	457	G
10/16/10	SKS	106.2	112.6	–58	–	–	–	N
03/06/11	SKS	214.9	110.2	15 ± 8.00	0.90 ± 0.12	46.1	–	G
03/10/11	S	116.4	44.8	14 ± 20.50	1.05 ± 0.47	117.2	508	F
04/03/11	SKS	104.1	107.6	–27 ± 18.00	0.31 ± 0.13	114.1	–	F

Note: The quality of measurements is rated as G (good), F (fair), and N (null).

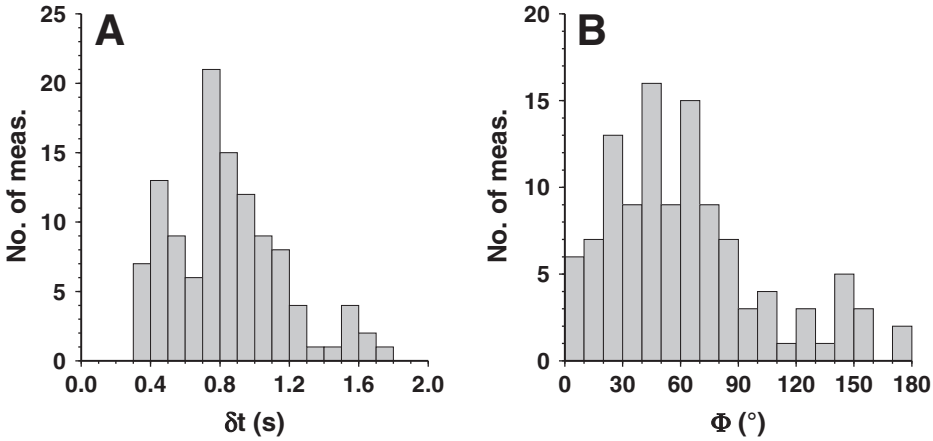

Figure 4. Histograms of (A) delay times and (B) fast polarization azimuths.

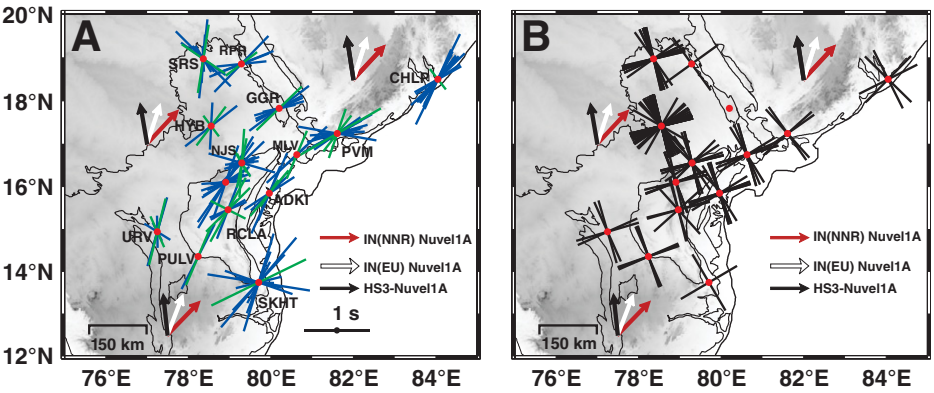

Figure 5. Map showing the individual (A) splitting and (B) null measurements at the station locations. The brown and white arrows represent the motion of the Indian plate in a no-net rotation frame and relative to a fixed Eurasian plate, respectively, as defined by the NUVEL1A plate model (DeMets et al., 1994). Black arrows represent the motion of the Indian plate in the HS3-NUVEL1A hotspot reference frame (Gripp and Gordan, 2002). (A) The orientation and length of the lines correspond to the fast polarization azimuth and delay time, respectively. Blue lines represent SK(K)S measurements, and green lines represent S-wave measurements. (B) The two arms of the cross for each null measurement indicate the back azimuth of the event and the corresponding potential null direction.

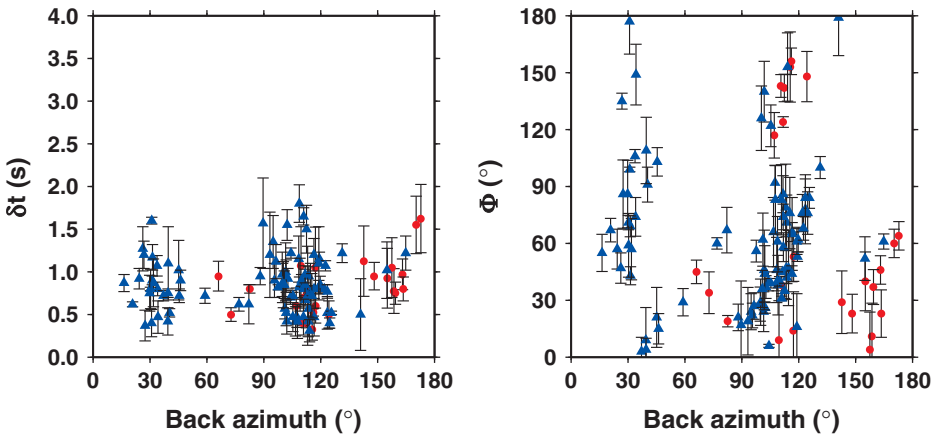

Figure 6. Plot showing the variation of (A) delay times (left) and (B) fast polarization azimuth (right) using direct S wave (red circles) and SK(K)S (blue triangles), plotted as a function of back azimuth. The measurement errors are shown as vertical bars.

are consistent at all the stations (Fig. 5B). For station HYB, the observed null measurements across the whole range of back azimuths are in good agreement with the apparent isotropic nature inferred from previous studies that suggest weaker or complex anisotropy (Chen and Ozalaybey, 1998; Barruol and Hoffmann, 1999; Heintz et al., 2009). The observed non-null measurement at HYB has significant Φ and δt variations with back azimuth; such a pattern implies a complex anisotropic structure beneath the station (Silver and Savage, 1994).

Our results show that the anisotropic directions in the Eastern Dharwar craton are predominantly oriented in the NNE-SSW and NE directions, with a few measurements suggesting NNW-SSE fast-axis azimuths. These directions appear to be aligned with plate-motion direction of the Indian plate with respect to Eurasia (DeMets et al., 1994). Interestingly, the splitting directions at stations in the vicinity of the east coast of India, which carries imprints of rifting during the Paleoproterozoic, follow its trend. It is postulated that the evolution of the Eastern Ghat mobile belt involved two distinct convergence episodes (Atlantic and Andean types) that were initiated by the onset of continental rifting at ca. 2 Ga along the eastern margin of the Indian plate and culminated as a continent-continent collision ca. 1.55 Ga (Kumar and Leelanandam, 2008). Given such a scenario, the splitting directions parallel to the coast suggest the presence of rift-parallel flow, akin to the observations in the Ribeira belt and Sao Frãncisco craton in SE Brazil. The large splitting times observed in SE Brazil were interpreted in terms of a combination of fossilized anisotropy in the lithospheric mantle and asthenospheric flow due to present-day plate motion (Heintz et al., 2003). In a similar fashion, the splitting trends in the vicinity of the Eastern Ghat mobile belt, albeit with smaller splitting times, can be explained by invoking both lithospheric and asthenospheric anisotropy, suggesting that the continental rifting could have occurred parallel to paleolithospheric structures.

In an attempt to isolate the effects of anisotropy frozen in the lithosphere and that due to active upper-mantle flow, we examined the variations in the apparent splitting measurements with back azimuth (Fig. 6) in terms of two layers. Since the number of splitting measurements at individual stations is grossly insufficient to test the presence of two-layer anisotropy, we combined the splitting measurements with similar back-azimuthal variation at all the stations after selecting the high-quality ones for which the error in fast polarization azimuth was less than 15°. As can be seen from Figure 6, large variations in

the splitting parameters, particularly the fast-axis azimuths, over a narrow range of back azimuths are uncharacteristic of a single layer of anisotropy and suggest multiple layers of anisotropy (Silver and Savage, 1994; Walker et al., 2004; Fontaine et al., 2007). We performed forward modeling to best explain the dependence of the splitting parameters on the incoming polarization (back azimuth in the case of SK[K]S) using two anisotropic layers with a horizontal axis of symmetry. Using the method of Silver and Savage (1994), the apparent splitting parameters were computed for a range of incoming polarizations by systematically varying the fast-axis azimuth and delay time of each of the layers for a dominant signal frequency of 6 s. The optimum model we found is characterized by $\Phi_{upper} = 58°$, $\delta t_{upper} = 0.3$ s, $\Phi_{lower} = 16°$, and $\delta t_{lower} = 0.8$ s. Since the delay time of 0.3 s for the upper layer is very small and can be considered as null and that for the lower layer is close to the average splitting time for the entire data set, we feel that shear at the base of the lithosphere is the dominant mechanism for forging anisotropy beneath the Eastern Dharwar craton, although the presence of multiple layers of anisotropy is likely.

CONCLUSIONS

In total, 113 new shear-wave splitting measurements were obtained in the Eastern Dharwar craton using SK(K)S and S waveforms registered at 14 broadband stations. The delay times between the fast and slow axes are clustered around 0.8 s, i.e., slightly lower than that observed globally for continental shields (~1 s). The fast polarization azimuths at a majority of stations are clustered in the NNE-SSW direction, in accordance with the present-day motion of the Indian plate as defined through the NUVEL1A model (DeMets et al., 1994). The anisotropy can be explained mostly by shear at the base of the lithosphere controlled by the topography on the lithosphere-asthenosphere boundary. The ENE-WSW orientation at a few stations is probably due to the effect of anisotropy frozen in the Indian subcontinental lithosphere while undergoing tectonic deformation. Although our observations are inconsistent with a single layer of anisotropy beneath the Dharwar craton, the anisotropy in the upper layer seems to be too small to invoke two layers of anisotropy. Interestingly, the fast axes of anisotropy in the vicinity of the Eastern Ghat mobile belt reveal a coast-parallel trend suggestive of a superposition of the effects of continental rifting along the eastern margin of the Indian plate and the strain at the base of the lithosphere due to the present-day plate motion.

ACKNOWLEDGMENTS

The Council of Scientific and Industrial Research has funded the networks that have been providing a wealth of seismological data. We are thankful to N.A. Teanby for the shear-wave splitting code. We sincerely thank the staff members of the Seismological Observatory, National Geophysical Research Institute, for their support in installation and maintenance of the networks. The editor and two reviewers are thanked for their insightful comments.

REFERENCES CITED

Anand, M., Gibson, S.A., Subba Rao, K.V., Kelley, S.P., and Dickin, A.P., 2003, Early Proterozoic melt generation processes beneath the intra-cratonic Cuddapah Basin, southern India: Journal of Petrology, v. 44, p. 2139–2171, doi:10.1093/petrology/egg073.

Babuška, V., and Cara, M., 1991, Seismic Anisotropy in the Earth: Dordrecht, Netherlands, Kluwer Academic Publishers, 217 p.

Babuška, V., Plomerova, J., and Sileny, J., 1993, Models of seismic anisotropy in the deep continental lithosphere: Physics of the Earth and Planetary Interiors, v. 78, p. 167–191, doi:10.1016/0031-9201(93)90154-2.

Balakrishnan, S., Hanson, G.N., and Rajamani, V., 1990, Pb and Nd isotope constraints on the origin of high Mg and tholeiitic amphibolites, Kolar schist belt, south India: Contributions to Mineralogy and Petrology, v. 107, p. 272–292.

Barruol, G., and Hoffmann, R., 1999, Upper mantle anisotropy beneath the Geoscope stations: Journal of Geophysical Research, v. 104, p. 10,757–10,773, doi:10.1029/1999JB900033.

Biswas, S.K., 2003, Regional tectonic framework of the Pranhita-Godavari Basin, India: Journal of Asian Earth Sciences, v. 21, p. 543–551, doi:10.1016/S1367-9120(02)00145-1.

Booth, D.C., Crampin, S., Evans, R., and Roberts, G., 1985, Shear-wave polarization near the North Anatolian fault—I. Evidence for anisotropy-induced shear-wave splitting: Geophysical Journal of the Royal Astronomical Society, v. 83, p. 61–73, doi:10.1111/j.1365-246X.1985.tb05156.x.

Bowman, J.R., and Ando, M., 1987, Shear-wave splitting in the upper-mantle wedge above the Tonga subduction zone: Geophysical Journal of the Royal Astronomical Society, v. 88, p. 25–41, doi:10.1111/j.1365-246X.1987.tb01367.x.

Chadwick, B., Vasudev, V.N., and Hegde, G.V., 2000, The Dharwar craton, southern India, interpreted as the result of Late Archaean oblique convergence: Precambrian Research, v. 99, p. 91–111, doi:10.1016/S0301-9268(99)00055-8.

Chen, W.P., and Ozalaybey, S., 1998, Correlation between seismic anisotropy and Bouguer gravity anomalies in Tibet and its implications for lithospheric structures: Geophysical Journal International, v. 135, p. 93–101, doi:10.1046/j.1365-246X.1998.00611.x.

Crampin, S., 1994, The fracture criticality of crustal rocks: Geophysical Journal International, v. 118, p. 428–438, doi:10.1111/j.1365-246X.1994.tb03974.x.

DeMets, C., Gordon, R.G., Argus, D.F., and Stein, S., 1994, Effect of recent revisions to the geomagnetic reversal time scale on estimate of current plate motions: Geophysical Research Letters, v. 21, p. 2191–2194, doi:10.1029/94GL02118.

Fontaine, F.R., Barruol, G., Tommasi, A., and Bokelmann, G.H.R., 2007, Upper-mantle flow beneath French Polynesia from shear wave splitting: Geophysical Journal International, v. 170, p. 1262–1288, doi:10.1111/j.1365-246X.2007.03475.x.

Fouch, M.J., and Rondenay, S., 2006, Seismic anisotropy beneath stable continental interiors: Physics of the Earth and Planetary Interiors, v. 158, p. 292–320.

Fu, Y.V., Chen, Y.J., Li, A., Zhou, S., Liang, X., Ye, G., Jin, G., Jiang, M., and Ning, J., 2008, Indian mantle corner flow at southern Tibet revealed by shear wave splitting measurements: Journal of Geophysical Research Letter, v. 35, L02308.

Garnero, E.J., Maupin, V., Lay, T., and Fouch, M.J., 2004, Variable azimuthal anisotropy in Earth's lowermost mantle: Science, v. 306, p. 259–261, doi:10.1126/science.1103411.

Gibb, R.A., and Thomas, M.D., 1976, Gravity signature of the fossil plate boundaries in the Canadian Shield: Nature, v. 262, p. 199–200, doi:10.1038/262199a0.

Gripp, A.E., and Gordan, R.G., 2002, Young tracks of hotspots and current plate velocities: Geophysical Journal International, v. 150, p. 321–361, doi:10.1046/j.1365-246X.2002.01627.x.

He, X., and Long, M.D., 2011, Lowermost mantle anisotropy beneath the northwestern Pacific: Evidence from PcS, ScS, SKS, and SKKS phases: Geochemistry Geophysics Geosystems, v. 12, Q12012, doi:10.1029/2011GC003779.

Heintz, M., Vauchez, A., Assumpcao, M., Barruol, G., and Egydio-Silva, M., 2003, Shear wave splitting in SE Brazil: An effect of active or fossil upper mantle flow, or both?: Earth and Planetary Science Letters, v. 211, p. 79–95, doi:10.1016/S0012-821X(03)00163-8.

Heintz, M., Kumar, P.V., Gaur, V.K., Priestley, K., and Rai, S.S., 2009, Anisotropy of the Indian continental lithospheric mantle: Geophysical Journal International, v. 179, p. 1341–1360, doi:10.1111/j.1365-246X.2009.04395.x.

Jayananda, M., Moyen, J.-F., Martin, H., Peucat, J.-J., Auvray, B., and Mahabaleswar, B., 2000, Late Archaean (2550–2520 Ma) juvenile magmatism in the Eastern Dharwar craton, southern India: Constraints from geochronology, Nd-Sr isotopes and whole rock geochemistry: Precambrian Research, v. 99, p. 225–254, doi:10.1016/S0301-9268(99)00063-7.

Kay, I., Sol, S., Kendall, J.-M., Thomson, C., White, D., Asudeh, B., Roberts, B., and Francis, D., 1999, Shear wave splitting observations in the Archean craton of Western Superior: Geophysical Research Letters, v. 26, p. 2669–2672, doi:10.1029/1999GL010493.

Kennett, B.L.N., and Engdahl, E.R., 1991, Travel times for global earthquake location and phase identification: Geophysical Journal International, v. 105, p. 429–465, doi:10.1111/j.1365-246X.1991.tb06724.x.

Kumar, A., Padma Kumari, V.M., Dayal, A.M., Murthy, D.S.N., and Gopalan, K., 1993, Rb-Sr ages of Proterozoic kimberlites of India: Evidence for contemporaneous emplacement: Precambrian Research, v. 62, p. 227–237, doi:10.1016/0301-9268(93)90023-U.

Kumar, K.V., and Leelanandam, C., 2008, Evolution of the Eastern Ghats belt, India: A plate tectonic perspective: Journal of the Geological Society of India, v. 72, p. 720–749.

Kumar, M.R., and Singh, A., 2008, Evidence for plate motion related strain in the Indian Shield from shear wave splitting measurements: Journal of Geophysical Research, v. 113, B08306, doi:10.1029/2007JB005128.

Kumar, N., Kumar, M.R., Singh, A., Raju, P.S., and Rao, N.P., 2010, Shear wave anisotropy of the Godavari rift in the south Indian Shield: Rift signature or APM related strain?: Physics of the Earth and Planetary Interiors, v. 181, p. 82–87, doi:10.1016/j.pepi.2010.05.002.

Kumar, P., Yuan, X., Kumar, M.R., Kind, R., Li, X., and Chadha, R.K., 2007, The rapid drift of the Indian tectonic plate: Nature, v. 449, p. 894–897, doi:10.1038/nature06214.

Long, M.D., 2009, Complex anisotropy in D″ beneath the eastern Pacific from SKS-SKKS splitting discrepancies: Earth and Planetary Science Letters, v. 283, p. 181–189, doi:10.1016/j.epsl.2009.04.019.

Mainprice, D., Barruol, G., and Ben Ismail, B., 2000, The seismic anisotropy of the Earth's mantle: From single crystal to polycrystal, *in* Karato, S., et al., eds., Earth's Deep Interior Mineral Physics and Tomography from the Atomic to the Global Scale: American Geophysical Union Geophysical Monograph 117, p. 237–264.

Mandal, P., 2011, Upper mantle seismic anisotropy in the intracontinental Kachchh rift zone, Gujrat, India: Tectonophysics, v. 509, p. 81–92, doi:10.1016/j.tecto.2011.05.013.

Maupin, V., Garnero, E.J., Lay, T., and Fouch, M.J., 2005, Azimuthal anisotropy in the D″ layer beneath the Caribbean: Journal of Geophysical Research, v. 110, B08301, doi:10.1029/2004JB003506.

Mitra, S., Priestley, K., Gaur, V.K., Rai, S.S., and Haines, J., 2006, Variation of Rayleigh wave group velocity dispersion and seismic heterogeneity of the Indian crust and uppermost mantle: Geophysical Journal International, v. 164, p. 88–98, doi:10.1111/j.1365-246X.2005.02837.x.

Nagaraja Rao, B.K., Rajurkar, S.T., Ramalingaswamy, G., and Ravindra Babu, B., 1987, Stratigraphy, structure and evolution of the Cuddapah Basin, *in* Radhakrishna, B.P., ed., Purana Basins of Peninsular India: Geological Society of India Memoir 6, p. 33–86.

Olsen, K.H., and Morgan, P., 1995, Introduction: Progress in understanding continental rifts, *in* Olsen, K.H., ed., Continental Rifts: Evolution, Structure, Tectonics: Amsterdam, Elsevier, Developments in Geotectonics, v. 25, p. 3–26.

Paul, D.K., Ray Barman, T., McNaughton, N.J., Fletcher, I.R., Potts, P.J., Ramakrishnan, M., and Augustine, P.F., 1990, Archean-Proterozoic evolution of India charnockites: Isotope and geochemical evidence for granulites of the Eastern Ghats belt: The Journal of Geology, v. 98, p. 253–263, doi:10.1086/629396.

Ramakrishnan, M., and Vaidyanadhan, R., 2008, Geology of India, Volume 1: Bangalore, Geological Society of India, 556 p.

Ramam, P.K., and Murty, V.N., 1997, Geology of Andhra Pradesh: Bangalore, India, Geological Society of India, 245 p.

Ramesh, D.S., and Prakasam, K.S., 1995, Shear wave splitting observations from the Indian Shield: Proceedings of the Indiana Academy of Sciences, v. 104, p. 85–114.

Ramesh, D.S., Bharthur, R.N., Prakasam, K.S., Srinagesh, D., Rai, S.S., and Gaur, V.K., 1996, Predominance of plate motion–related strain in the south Indian Shield: Current Science, v. 70, p. 843–847.

Saikia, D., Kumar, M.R., Singh, A., Mohan, G., and Dattatrayam, R.S., 2010, Seismic anisotropy beneath the Indian continent from splitting of direct S wave: Journal of Geophysical Research, v. 115, B12315, doi:10.1029/2009JB007009.

Sandvol, E., Ni, J., Kind, R., and Zhao, W., 1997, Seismic anisotropy beneath the southern Himalayas–Tibet collision zone: Journal of Geophysical Research, v. 102, p. 17,813–17,823, doi:10.1029/97JB01424.

Savage, M.K., 1999, Seismic anisotropy and mantle deformation: What have we learned from shear wave splitting?: Reviews of Geophysics, v. 37, p. 65–106, doi:10.1029/98RG02075.

Silver, P.G., 1996, Seismic anisotropy beneath the continents: Probing the depths of geology: Annual Review of Earth and Planetary Sciences, v. 24, p. 385–432, doi:10.1146/annurev.earth.24.1.385.

Silver, P.G., and Chan, W.W., 1991, Shear-wave splitting and sub-continental mantle deformation: Journal of Geophysical Research, v. 96, p. 16,429–16,454, doi:10.1029/91JB00899.

Silver, P.G., and Savage, M.K., 1994, The interpretation of shear-wave splitting parameters in the presence of two anisotropic layers: Geophysical Journal International, v. 119, p. 949–963, doi:10.1111/j.1365-246X.1994.tb04027.x.

Singh, A., Kumar, M.R., Raju, P.S., and Ramesh, D.S., 2006, Shear wave anisotropy of the northeast Indian lithosphere: Geophysical Research Letters, v. 33, L16302, doi:10.1029/2006GL026106.

Singh, A., Kumar, M.R., and Raju, P.S., 2007, Mantle deformation in Sikkim and adjoining Himalaya: Evidences for a complex flow pattern: Physics of the Earth and Planetary Interiors, v. 164, p. 232–241, doi:10.1016/j.pepi.2007.07.003.

Teanby, N.A., Kendall, J.-M., and Baan, M.V.D., 2004, Automation of shear-wave splitting measurements using cluster analysis: Bulletin of the Seismological Society of America, v. 94, p. 453–463, doi:10.1785/0120030123.

Vasudev, V.N., Chadwick, B., Nutman, A.P., and Hedge, G.V., 2000, Rapid development of Late Archean Hutti schist belt, northern Karnataka: Implications of new field data and SHRIMP U/Pb zircon ages: Journal of the Geological Society of India, v. 55, p. 529–540.

Walker, K.T., Nyblade, A.A., Klemperer, S.L., Bokelmann, G.H.R., and Owens, T.J., 2004, On the relationship between extension and anisotropy: Constraints from shear wave splitting across the East African Plateau: Journal of Geophysical Research, v. 109, B08302, doi:10.1029/2003JB002866.

Wookey, J., and Kendall, J.M., 2004, Evidence of midmantle anisotropy from shear wave splitting and the influence of shear-couple P waves: Journal of Geophysical Research, v. 109, B07309, doi:10.1029/2003JB002871.

Wüstefeld, A., Bokelmann, G., Zaroli, C., and Barruol, G., 2008, SplitLab: A shear-wave splitting environment in Matlab: Computers & Geosciences, v. 34, p. 515–528, doi:10.1016/j.cageo.2007.08.002.

MANUSCRIPT RECEIVED 13 JANUARY 2012
REVISED MANUSCRIPT RECEIVED 13 MARCH 2012
MANUSCRIPT ACCEPTED 14 MARCH 2012

Printed in the USA